Proceedings Paper:
Hayajneh, A, Zaidi, SAR, Hafeez, M et al. (2 more authors) (2019) Coverage Analysis of Drone-Assisted Backscatter Communication for IoT Sensor Network. In: Workshop on Wireless sensors and Drones in Internet of Things (Wi-DroIT 2019). Wi-DroIT 2019 (in conjunction with DCOSS 2019), 29-31 May 2019, Santorini Island, Greece. IEEE , pp. 584-590. ISBN 978-1-7281-0570-3

https://doi.org/10.1109/DCOSS.2019.00108

Coverage Analysis of Drone-Assisted Backscatter Communication for IoT Sensor Network

Ali Hayajneh, Syed Ali Raza Zaidi, Maryam Hafeez, Des McLernon and Moe Win

***Abstract*—In this article, we develop a comprehensive framework to characterize the performance of drone assisted Backscatter communication based Internet of things (IoT) sensor network. We consider a scenario such where drone transmits RF carrier which is modulated by IoT sensor node (SN) to transmit its data. The SN implements load modulation which results in amplitude shift keying (ASK) type modulation for the impinging RF carrier. In order to quantify the performance of considered network, we characterize the coverage probability for the ground based SN node. The statistical framework developed to quantify the coverage probability explicitly accommodates dyadic backscatter channel which experiences deeper fades than that of the one-way Rayleigh channel. Our model also incorporates Line of Sight (LoS) and Non-LoS (NLoS) propogation states for accurately modeling large-scale path-loss between drone and SN. We consider spatially distributed SNs which can be modelled using spatial Binomial Point process (BPP). We practically implement the proposed system using Software Defined Radio (SDR) and a custom designed SN tag. The measurements of parameters such as noise figure, tag reflection coefficient etc., are used to parametrize the developed framework. Lastly, we demonstrate that there exists an optimal set of parameters which maximizes the coverage probability for the SN.**

***Index Terms*—Drone, Backscatter communication, Dyadic fading, Stochastic geometry, Binomial process, Coverage probability.**

I. Introduction

The number of connected consumer electronic devices has exponentially increased over the past few years. According to recent statistics [1], there are already 19.4 billion internet connected devices that are in use across the globe, with the number of Internet-of-Things (IoT) devices currently around 8.3 billion. The number of IoT devices is expected to increase at a startling compound annual growth rate (CAGR) of 10%. With such massive volume of devices, it is becoming increasingly important to explore energy efficient (EE) IoT Sensor Node (SN) design. This is mainly motivated by the fact that recharging the deployed SNs individually on regular basis might be impractical, especially for those SNs which have limited post-deployment accessibility.

To realize EE design for IoT SNs, there are two possible avenues which have gained significant interest from research community: (i) develop energy optimal protocols/architecture for communication; (ii) harvest energy from ambient natural/synthetic sources to power the communication hardware. In recent past [2], there has been a significant interest in simultaneous wireless power and information transfer (SWIPT) based SN design. The SWIPT techniques employ rectenna, i.e., an antenna and a diode to charge an on board energy storage component (such as battery or a super-capacitor). The harvested power is in turn employed for provisioning communication between the SN and the intended access point (AP). The key limitation of SWIPT is that the harvested power is very small and the RF signals which are optimal for energy harvesting are not necessarily optimal for communication.

RF Backscatter based communication [3]–[6] presents an attractive alternative. Backscatter radio communication does not require expensive active components such as as RF oscillators, mixers, crystals and decoupling capacitors etc. The SNs communicate with AP (also called Reader) by modulating the ambient un-modulated RF carrier which is transmitted by the AP. The RF carrier modulation is achieved by connecting an antenna to different loads which fundamentally translates into different antenna-load reflection coefficients. Interested readers are directed to [1] for a recent tutorial which provides a comprehensive coverage of the backscatter based SN design. RF backscatter based IoT SNs are particularly well suited for applications where periodic polling can be employed for SN data aggregation/collection. In other words, the data collection can be duty cycled by the reader in an adaptive manner. This is particularly useful in multi-modal sensing where certain knowledge at the reader can be employed to increase/decrease the duty cycle of data collection. For instance, in smart agriculture application, weather data can be exploited to duty cycle the collection of reading from soil moisture sensors. RF backscatter based IoT SNs are particularly well suited to environmental monitoring applications where SNs are spread across a wider geographical region. Our prime interest in RF backscatter based SNs is in the context of smart agriculture where such sensors can provide wide scale deployment at a very low cost. In practice, it is possible to print these sensors (either using conductive ink on paper or on the semiconductor substrate) and mount a single chip to implement a SN node. Some initial investigations on backscatter based SNs for soil moisture monitoring are conducted in [5], [7]–[9].

The key issue with the traditional approaches is that the coverage range for RF backscatter based SNs is only of the order of few hundred meters at best. Consequently, a dense deployment of readers is required for provisioning data collection which is costly, as this requires not only more hard-

A. Hayajneh, S. A. R. Zaidi, Des. C. McLernon are with the School of Electronic and Electrical Engineering, University of Leeds, Leeds, LS2 9JT, United Kingdom, e-mail: {elamh,s.a.zaidi,d.c.mclernon}@leeds.ac.uk. Maryam Hafeez is with School of Computing and Engineering, University of Huddersfield, Huddersfield, HD1 3DH, United Kingdom, e-mail: M.Hafeez@hud.ac.uk. Moe Win is with the Laboratory for Information and Decision Systems, Massachusetts Institute of Technology, Cambridge, MA 02139 USA, e-mail: moewin@mit.edu. This research is supported by the Research England Global Research Challenges Fund and National Science Foundation under Grant CCF-1525705.

ware but also post-deployment maintenance. A simple solution would be to use a single RF reader which is mounted on a mobile platform which can navigate the intended monitoring area. Drones present an attractive choice for mounting the backscattering reader as several farmers are using drones for various other agricultural monitoring functions. For instance, multi-spectral cameras mounted on drones are being used to calculate vegetation indices (for instance Normalized Differential Vegetation Index (NDVI)) which highlight a particular characteristic of vegetation. To this end, this paper explores the performance of RF Backscatter based IoT SNs with a drone mounted flying Reader (DFR).

A. Contributions

In order to fully understand networking dynamics of backscatter based IoT SN served by the DFR, it is essential to characterize both the link and the network level performance of such deployments. To this end, in this paper, we aim to develop a comprehensive statistical framework to characterize the performance of considered IoT SN. To the best of our knowledge this is first study which presents such a statistical framework to characterize performance of drone assisted backscatter based IoT SNs. The performance of SNs is measured and quantified in terms of the well known coverage probability metric. The coverage probability is defined as the probability that the received signal-to-noise-ratio (SNR) exceeds a certain desired threshold. The threshold can easily be selected to satisfy a certain desired bit-error-rate (BER), i.e. coverage probability can essentially serve as a proxy of successful packet decoding probability. The framework presented in this paper implicitly incorporates realistic propagation dynamics of communication between DFR and SNs by: (i) employing the large-scale path-loss model which accommodate both Line-of-Sight (LoS) and Non-LoS (NLoS) link states; and (ii) by employing the small-scale fading model which captures the dyadic nature of backscatter communication, i.e., forward propagation (from DFR-to-SN) and backward propagation (SN-to-DFR) may experience non-zero correlation[1]. Due to dyadic Rayleigh fading channel, it is difficult to analyse the performance of randomly scattered SNs[2]. However, we present alternative closed-form expressions which are amenable to analysis. We practically implement a tag and software-defined radio (SDR) based reader and parametrize the developed framework to investigate the coverage performance of SNs. Lastly, impact of various parametric variations and optimal dimensioning of the network is briefly explored.

B. Organization

The rest of the paper is organized as follows: Section II introduces the system model and deployment geometry of the network. Section III gives the performance analysis and mathematical modelling. Section IV presents numerical results. Finally, Section V provides some future work and conclusions.

[1]Notice that due to dyadic fading channel, the analysis of performance is different from the scenario ([10], [11]) where drone is used as a BS.

[2]We borrow tools from stochastic geometry for analysis. Interested reader is directed to [**?**] for a comprehensive tutorial.

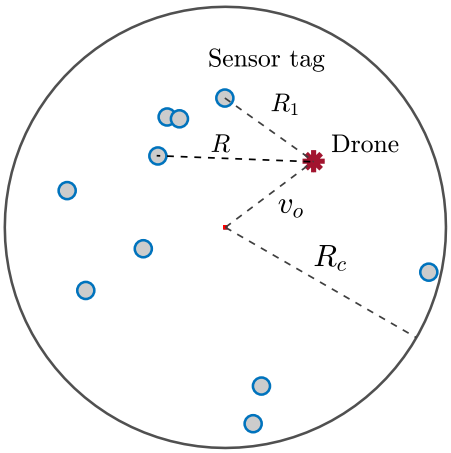

Fig. 1: Drone-assisted smart IoT agriculture geometry. A snapshot of the distribution of 10 sensor tags on the circular area of a radius R_c.

C. Notation.

Throughout this paper, we employ the following mathematical notations. The probability density function (PDF) of a random variable X is represented as $f_{\mathrm{X}}(x)$ with the cumulative density function (CDF) written as $F_{\mathrm{X}}(x)$. The expectation of a function $g(X)$ of a random variable X is represented as $\mathbb{E}_{\mathrm{X}}[g(X)]$. The bold-face lower case letters (e.g., $\mathbf{x}$) are employed to denote a vector in $\mathbb{R}^2$ and $\|\mathbf{x}\|$ is its Euclidean norm.

II. System Model

A. Spatial and Network Models

As depicted in Figure 1, we consider a scenario where a drone is employed for data aggregation from SN tags. The drone is furnished with a mono-static SN tag reader and is tasked to cover a desired service area which is modelled by a disc of radius R_{c}. It is assumed that SN tags are uniformly distributed in the intended service area. The reader does not possess any prior knowledge about the tag location and randomly moves across the area such that its reference distance to the center of the disc is v_{o}[3]. Assuming that the number of SNs is finite and fixed, the spatial distribution of the SNs is captured by a binomial point process (BPP) such that [12]:

$$\Phi = \{\mathbf{x}_0, \mathbf{x}_1, ..., \mathbf{x}_{\mathrm{N_s}}, \forall\ \mathbf{x}_{\mathrm{i}} \in \mathbb{R}^2\}, \tag{1}$$

where N_{s} is the number of tags on the two dimensional set space. At a particular time instance, only one SN is served on a particular resource channel to avoid co-channel interference. The sensor at the location $\mathbf{x}_{\mathrm{i}}$ is associated to the nearest neighbour flying drone reader.

[3]For randomly chosen point inside the circular coverage area, v_{o} is no longer constant and is indeed a random variable, say V_o with PDF given by $f_{\mathrm{V_o}}(v_{\mathrm{o}}) = \frac{2v_{\mathrm{o}}}{R_{\mathrm{c}}^2}$, for $v_{\mathrm{o}} \in [0, R_{\mathrm{c}}]$.

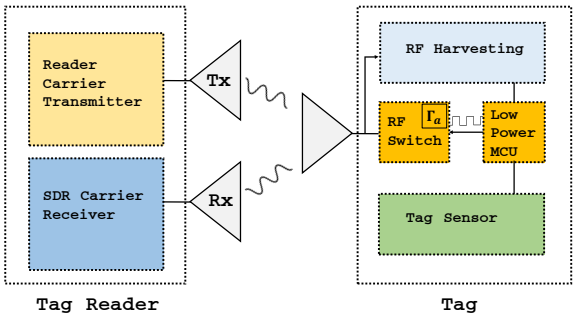

Fig. 2: Architecture of backscatter DFR and SN.

B. SN Tag and DFR's SDR Implementation

The backscattering SN tag reflects the ambient RF carrier transmitted by the DFR by modulating the antenna's reflection coefficient. This is simply achieved by connecting the antenna to two different loads (one for 0 information bit and the other for 1 bit). In our SN design, the load modulation is driven by the serial payload data packets generated by ultra-low power microcontroller unit (MCU). Either MSP430 from Texas Instrument or STM32L063R8 ARM M0+ are suitable as their power-consumption is several μ-Amperes in different modes. In our reference implementation the tag charges a super-capacitor by harvesting energy from RF carrier. The harvested power is used to drive the SN MCU. In a nutshell, our load modulation scheme translates to amplitude shift keying (ASK). We associate the higher reflection coefficient $\Gamma_{\rm a}$ to the binary logic 0 and design a circuit which tries to minimize reflection coffecient for binary logic 1 (i.e., no reflected carrier for the 1 binary logic). Hence, if the binary logic 1 has a reflection coefficient $\Gamma_0 = 0$, the resulting tag transmit signal can be written as [4]:

$$x_{\rm Tag}(t) = \begin{cases} \Gamma_{\rm a} b_{\rm n}(t - nT), & \text{Logic 0} \\ 0, & \text{Logic 1}, \end{cases} \tag{2}$$

for $t \in [nT, (n+1)nT]$, where $\mathrm{n}(t - nT)$ is the information bit of a duration T. Figure 3 depicts the reception and decoding of a serial data with the payload word "OK" in our reference implementation. The carrier is generated by the Nuand BladeRF SDR transceiver with the transmit power of 14 dBm. The bottom blue waveform presents the received modulated carrier of a bit rate of 2.4 Kb/s. As we can see, the reflection coefficient affects the distance between the two binary levels of the modulated carries and this directly effects the choice of constellation size [4] and the likelihood of correct demodulation (i.e., the bit error rate of the communication link). The red bit sequence is the decoded bits after performing level detection on the bandpass received RF signal and then recovering the clock utilizing Mueller-Müller timing recovery scheme [13].

[4]It is envisioned that higher order modulation can be implemented by employing cascaded RF switches

C. Large-Scale fading Model:

In order to accurately capture the propagation conditions for drone assisted backscatter communication, we employ the path-loss model presented in [14]. The backscatter communication link is dyadic in nature, i.e. it is characterized by the product of forward (DFR-to-SN) and backward (SN-to-DFR) channel gains. We assume both forward and backward channel experience same path-loss, which is reasonable for the mono-static architecture. The employed path-loss model adequately captures LoS and NLoS contributions for drone-to-ground communication as follows:

$$L_{\rm LoS}(h_{\rm d}, r) = K_{\rm LoS}\Big(r^2 + h_{\rm d}^2\Big), \tag{3}$$

$$L_{\rm NLoS}(h_{\rm d}, r) = K_{\rm NLoS}\Big(r^2 + h_{\rm d}^2\Big), \tag{4}$$

where $h_{\rm d}$ is the height of the drone in meters, r is the two dimensional projection separation between the drone and the SN, $K_{\rm LoS}$ and $K_{\rm NLoS}$ are environment and frequency dependent parameters such that $K_{\rm i} = \zeta_{\rm i}\left(c/(4\pi f_{\rm MHz})\right)^{-1}$, $\zeta_{\rm i}$ is the excess path-loss for $i \in \{LoS, NLoS\}$ with typical values for urban areas $\zeta_{\rm LoS} = 1$ dB. The probabilites of having a LoS and NLoS link between the DFR to the desired SN are as follows:

$$\mathcal{P}_{\rm LoS}(h_{\rm d}, r) = \frac{1}{1 + a\,\mathrm{e}^{-b\eta\,\tan^{-1}\left(\frac{r}{h_{\rm d}}\right) + b\,a}}, \tag{5a}$$

$$\mathcal{P}_{\rm NLoS}(h_{\rm d}, r) = 1 - \mathcal{P}_{\rm LoS}(h_{\rm d}, r), \tag{5b}$$

where a, b, c are environment dependent constants, $\eta = 180/\pi$ and θ is the elevation angle in degrees.

D. Small-Scale Dyadic Rayleigh Fading Channel

We consider a mono-static backscattering DFR where both transmit and receive antennas are co-located as shown in Figure 2. The DFR transmits an unmodulated RF carrier and the SN tag reflects it back with a reflection coefficient of $\Gamma_{\rm a}$. Both forward ($\mathcal{G}_{\rm f}$) and backward ($\mathcal{G}_{\rm b}$) propagation channels suffer from Rayleigh flat fading. However, due to the dyadic nature of the link, the channels have non-zero correlation captured by the parameter $\rho = \mathbb{E}(\mathcal{G}_{\rm f}, \mathcal{G}_{\rm b})$ with $\mathcal{G}_{\rm f}, \mathcal{G}_{\rm b} \sim \mathcal{CN}(0, 1)$. The received channel power gain is given by $\mathcal{H}_{\rm f} = \|\mathcal{G}_{\rm f}\|^2$ and $\mathcal{H}_{\rm b} = \|\mathcal{G}_{\rm b}\|^2$ and has the joint distribution as:

$$\begin{aligned} f_{\mathcal{H}_{\rm f},\mathcal{H}_{\rm b}}(h_{\rm f}, h_{\rm f}; \rho) \;=\; & \frac{2}{\tilde{\rho}\sigma_{\rm f}^2\sigma_{\rm b}^2} \exp\left(-\frac{1}{\tilde{\rho}}\left[\frac{h_{\rm f}}{\sigma_{\rm f}^2} + \frac{h_{\rm b}}{\sigma_{\rm b}^2}\right]\right) \\ & \times \mathcal{I}_o\left(\frac{\rho\sqrt{h_{\rm f} h_{\rm b}}}{(1-\rho^2)\sigma_{\rm f}^2\sigma_{\rm b}^2}\right), \end{aligned} \tag{6}$$

where $\mathcal{I}_o(z) = \frac{1}{\pi}\int_0^{\pi} \exp\big(-z\cos(t)\big)\,\mathrm{d}t$, is the modified Bessel function of first kind and zero order, $\tilde{\rho} = 1 - \rho^2$, $\sigma_{\rm f}^2$ and $\sigma_{\rm b}^2$ are the variances of $\mathcal{G}_{\rm f}$ and $\mathcal{G}_{\rm b}$ respectively. The PDF of the equivalent dyadic fading channel coefficient $\mathcal{H} = \mathcal{H}_{\rm f}\mathcal{H}_{\rm b}$ can be written as

$$f_{\mathcal{H}}(h, \rho) = \frac{1}{2\tilde{\rho}\sigma_{\rm f}^2\sigma_{\rm b}^2} \mathcal{I}_o\left(\frac{\rho\sqrt{h}}{\tilde{\rho}\sigma_{\rm f}\sigma_{\rm b}}\right) \mathcal{K}_o\left(\frac{\rho\sqrt{h}}{\tilde{\rho}\sigma_{\rm f}\sigma_{\rm b}}\right), \tag{7}$$

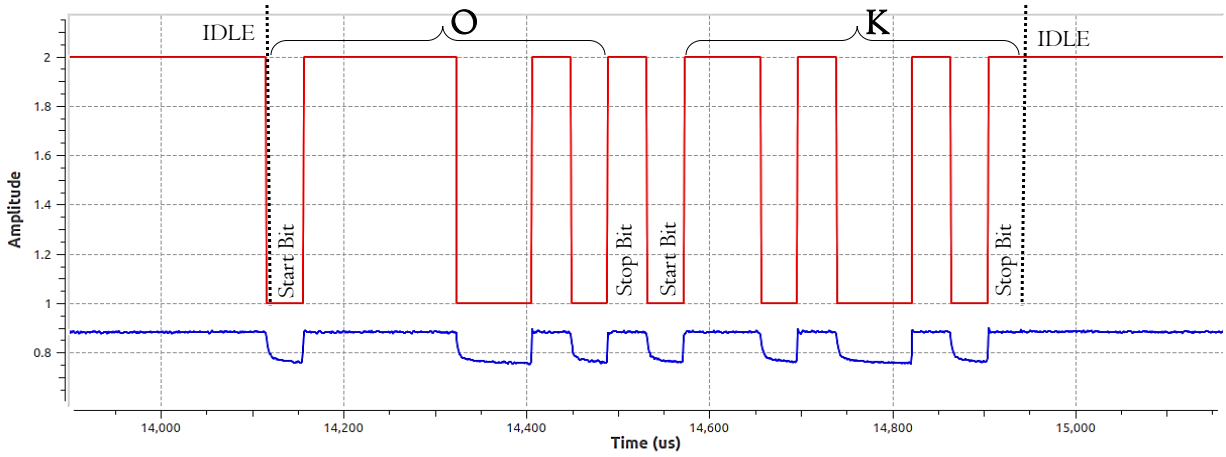

Fig. 3: Backscatter transmission of the serial data for the word "OK" which is equivalent to the hexadecimal representation of "0x4F,0x4B" from a sensor node tag. The lower curve is the ASK modulated carrier at the reader antenna. Serial data bit rate is 2.4 Kb/s.

where $\mathcal{K}_o(z) = \int_0^\infty \cos(z\sinh(t))\,\mathrm{d}t$, is the modified Bessel function of second kind and zero order. The PDF in (7) can be simplified as both forward and backward Rayleigh channels have unit mean,i.e., $\mathbb{E}(\mathcal{H}_\mathrm{f}) = \mathbb{E}(\mathcal{H}_\mathrm{b}) = 1$, as follows:

$$f_{\mathcal{H}}(h,\rho) = \frac{2}{\tilde{\rho}}\mathcal{I}_o\left(\frac{2\rho\sqrt{h}}{\tilde{\rho}}\right)\mathcal{K}_o\left(\frac{2\rho\sqrt{h}}{\tilde{\rho}}\right). \tag{8}$$

Obtaining a CDF for (8) which is required for the coverage analysis is quite complicated and mathematically intractable. Hence, we develop an alternative performance characterization framework by developing a tight approximation for the PDF in (8). In fact, (8) is a monotonically decreasing product of two modified Bessel functions in the interval $\mathcal{H} \in (0,\infty)$ as demonstrated in [15]. Moreover, the product decreases exponentially fast. Clearly, this motivates approximation of PDF by using asymptotic expressions for Bessel functions. The asymptotic Hankel expansion of the Bessle functions $\mathcal{I}_o(z)$ and $\mathcal{K}_o(z)$ is given as:

$$\mathcal{K}_o(z) \approx \frac{\sqrt{\pi}}{2}\exp(-z), \tag{9}$$

$$\mathcal{I}_o(z) \approx \frac{1}{z\sqrt{2\pi}}\exp(z). \tag{10}$$

Substituting the above to obtain $\tilde{f}_{\mathcal{H}}(h)$ and normalizing the result with the factor $c = \int_0^\infty \tilde{f}_{\mathcal{H}}(h)\,\mathrm{d}h$, we can write the approximate PDF as

$$\text{PDF:}\quad f_{\mathcal{H}}(h,\rho) \approx \frac{h^{-\frac{1}{2}}}{2\sqrt{\rho}}\exp\left(-\frac{2(1-\rho)\sqrt{h}}{1-\rho^2}\right) \tag{11}$$

$$\text{CDF:}\quad F_{\mathcal{H}}(h,\rho) \approx 1-\exp\left(-\frac{2(1-\rho)\sqrt{h}}{1-\rho^2}\right). \tag{12}$$

Figure 4 presents the tightness of the derived approximation in (12). It is evident that the approximation is very tight especially for high values of the correlation coefficient ρ. Combining large-scale and small scale fading model the overall propagation channel is given by $\mathcal{H}L(h_\mathrm{d},r)^{-2}$ with $\mathcal{H} = \mathcal{H}_\mathrm{f}\mathcal{H}_\mathrm{b}$ and $L(h_\mathrm{d},r) = L_{\mathrm{LoS}}(h_\mathrm{d},r)\mathcal{P}_{\mathrm{LoS}}(h_\mathrm{d},r) + L_{\mathrm{NLoS}}(h_\mathrm{d},r)\mathcal{P}_{\mathrm{NLoS}}(h_\mathrm{d},r)$.

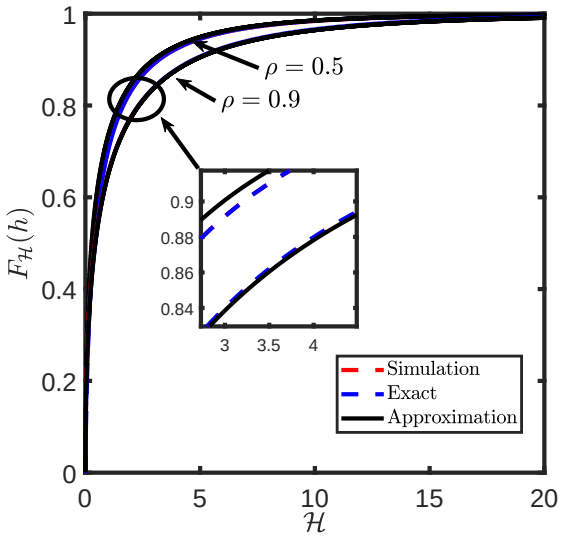

Fig. 4: Cumulative distribution function for the backscatter dyadic fading channel coefficient $\mathcal{H}$.

III. Performance Analysis

A. Link Distance Analysis

In this section, we characterize link distance distributions which are required to quantify the large scale path-loss given by (3). These distributions are employed to quantify coverage probability in section III-B. The PDF for the distance R from the DFR (located at distance v_o from the center of coverage region) to an arbitrary SN tag can be written as in (16). Employing the derived PDF with order-statistics enable derivation of the PDF of distance to nearest SN from DFR denoted by R_1 as summarized in Proposition 1.

Proposition 1. *The PDF of the distance R_1 from the DFR at distance v_o from the centre of the intended coverage area to the nearest SN tag can be evaluated as in* (18) *in the next page.*

Proof. Let N_s tags be distributed uniformly inside a circle of radius R_c. Then the derivation of the nearest neighbour distribution amongst the N_s SN tags follows the order statistics using the fact that for general N_s i.i.d random variables $Z_i \in \{Z_1, Z_2, ..., Z_{N_s}\}$ with PDFs $f_{Z_i}(z)$ ordered in ascending order. Then the PDF of $Z_1 = \min_i(Z_i)$ can be written as $f_{Z_1}(z) = N\left(1 - F_{Z_i}(z)\right)^{N-1} f_{Z_i}(z)$ [16]. Then, by applying this to (16), we can write the PDF of the distance R_1 as

$$f_{R_1}(r_1|v_o, R_c) = \begin{cases} f^{(1)}_{R_1}(r_1|v_o, R_c), & 0 \le r_1 \le R_c - v_o \\ f^{(2)}_{R_1}(r_1|v_o, R_c), & R_c - v_o < r_1 \le R_c + v_o, \end{cases} \tag{13}$$

where

$$f^{(1)}_{R_1}(r_1|v_o, R_c) = N_s(1 - F^{(1)}_R(r_1|v_o))^{N_s-1} f^{(1)}_R(r_1|v_o) \tag{14}$$

$$f^{(2)}_{R_1}(r_1|v_o, R_c) = N_s(1 - F^{(2)}_R(r|v_o))^{N_s-1} f^{(2)}_R(r_1|v_o). \tag{15}$$

■

From the previous proposition we can easily integrate $f_{R_1}(r_1|v_o, R_c)$ in (18) to get the CDF of the nearest neighbour distance distribution as

$$F_{R_1}(r_1|v_o, R_c) = \begin{cases} (1 - F^{(1)}_R(r_1|v_o, R_c))^{N_s}, & 0 \le r \le R_c - v_o \\ (1 - F^{(2)}_R(r_1|v_o, R_c))^{N_s}, & R_c - v_o < r \le R_c + v_o. \end{cases} \tag{19}$$

B. Coverage Probability

The coverage probability is defined as the probability that the SNR will be greater than a certain predefined value β. The average SNR for the uplink DFR can be quantified as:

$$\text{SNR} = \underbrace{\frac{P_t \mathcal{H}_f \mathcal{H}_b \Gamma_a [L_{LoS}(r_1)]^{-2}}{\sigma^2_N} \mathcal{P}_{LoS}(r_1)}_{\text{SNR}_L} + \underbrace{\frac{P_t \mathcal{H}_f \mathcal{H}_b \Gamma_a [L_{NLoS}(r_1)]^{-2}}{\sigma^2_N} \mathcal{P}_{NLoS}(r_1)}_{\text{SNR}_{NL}}, \tag{20}$$

where P_t is the reader's transmit power, σ^2_N is the additive white Gaussian noise (AWGN) power, SNR_L is SNR when there is a LoS link between the user and the BS, SNR_{NL} is SNR when there is a NLoS link between the user and the DFR. The coverage probability for any arbitrary mobile user can be evaluated as in the following theorem.

Proposition 2. (Coverage probability). *The coverage probability for any BPP with N_s SNs in the presence of AWGN can be evaluated as shown in* (21)*.*

Proof. Let a pre-defined threshold β of SNR, then the coverage probability can be defined as

$$\begin{aligned} P_c(\beta|v_o) &= P_r[\text{SNR} \ge \beta], \\ &= \mathbb{E}_{r_1}\left[1 - F_{\mathcal{H}}(\beta\sigma^2_N [L_L(r_1)]^2 / P_t \Gamma_a, \rho)\right] \mathcal{P}_L(r_1) \\ &+ \mathbb{E}_{r_1}\left[1 - F_{\mathcal{H}}(\beta\sigma^2_N [L_{NL}(r_1)]^2 / P_t \Gamma_a, \rho)\right] \mathcal{P}_{NL}(r_1). \end{aligned} \tag{22}$$

Hence, by evaluating the averaging operator in (22) with the distribution of R_1 in (18), we can quantify the coverage probability as shown in (21). ■

IV. Results and Discussion

In this section, we validate the developed statistical framework for quantifying the coverage probability. We also briefly explore the impact of different parametric variations on the coverage probability. We assume a rural environment with the parameters $a = 9.6$, $b = 0.28$ for the path-loss model (see Section 2), noise power $\sigma^2_N = 110$ dBm, $P_t = 0$ dB and $f = 915$ MHz illuminator carrier frequency. Also, as described in the previous sections, we consider Rayleigh flat wireless correlated fading channels. The noise power is estimated from the practical implementation of the system as described in Section II-B.

Figure 5(a) shows the coverage probability P_c versus the DFR height h_d for different tag reflection coefficient Γ_a and different reference locations v_o of the drone inside the coverage area. The Figure shows that, for a certain deployment parameters, there is always an optimal height of the DFR that maximizes the coverage probability and this optimal height changes with the change in the location of drone, i.e., with the change in v_o. For example, at $v_o = 0$ and $\Gamma_a = 0.9$, the optimal drone height is in the range of $40 - 60$ meters while for $v_o = 500$ and $\Gamma_a = 0.9$, the optimal height is lower in the range of $50 - 60$ meters. An interesting observation that follows Figure 5(a) is that the range of heights which optimize the coverage widens with increase in the reflection coefficient Γ_a. Moreover, the decrease in the coverage probability with the increase in DFR altitude (beyond optimal operational altitude) is much slower for higher reflection coefficient. Consequently, when reflection coefficient of tag is appropriately designed optimal height can be reduced while concurrently the SN coverage probability can be maximized.

Figure 5(b) studies coverage against increasing number of deployed SNs for different values of β. The figure shows that, as we increase the number of the deployed SNs, the coverage probability will increase. This is due to the change of the characteristics of the nearest neighbour SN distance distribution (i.e., the distance to the nearest neighbour SN becomes lower and hence the path-loss decreases). However, this is only true if the SNs do not interfere with each other, i.e., by employing highly directional antenna at DF. In practice, the increasing number of SNs contribute to co-channel interference and therefore reduce coverage probability.

Figure 5(c) shows the coverage probability against the DFR distance v_o from the center of the coverage area. As we describes before, the coverage probability decreases as the

$$f_{\mathrm{R}}(r|v_{\mathrm{o}},R_{\mathrm{c}})=\begin{cases} f_{\mathrm{R}}^{(1)}(r|v_{\mathrm{o}},R_{\mathrm{c}})=\frac{2r}{R_{\mathrm{c}}^2}, & 0\le r\le R_{\mathrm{c}}-v_{\mathrm{o}} \\ f_{\mathrm{R}}^{(2)}(r|v_{\mathrm{o}},R_{\mathrm{c}})=\frac{2r}{\pi R_{\mathrm{c}}^2}\arccos\left(\frac{r^2+v_{\mathrm{o}}^2-R_{\mathrm{c}}^2}{2v_{\mathrm{o}}r}\right), & R_{\mathrm{c}}-v_{\mathrm{o}}<r\le R_{\mathrm{c}}+v_{\mathrm{o}}, \end{cases} \tag{16}$$

with the CDF as follows:

$$F_{\mathrm{R}}(r|v_{\mathrm{o}})=\begin{cases} F_{\mathrm{R}}^{(1)}(r|v_{\mathrm{o}})=\frac{r^2}{R_{\mathrm{c}}^2}, & 0\le r\le R_{\mathrm{c}}-v_{\mathrm{o}} \\ F_{\mathrm{R}}^{(2)}(r|v_{\mathrm{o}})=\frac{r^2}{\pi R_{\mathrm{c}}^2}\left(\theta_1-\frac{1}{2}\sin\left(2\,\theta_1\right)\right)+\frac{1}{\pi}\left(\theta_2-\frac{1}{2}\sin\left(2\,\theta_2\right)\right), & R_{\mathrm{c}}-v_{\mathrm{o}}<r\le R_{\mathrm{c}}+v_{\mathrm{o}}, \end{cases} \tag{17}$$

with $\theta_1=\arccos\left(\frac{r^2-R_{\mathrm{c}}^2+v_{\mathrm{o}}}{2v_{\mathrm{o}}r}\right)$ and $\theta_2=\arccos\left(\frac{-r^2+R_{\mathrm{c}}^2+v_{\mathrm{o}}}{2v_{\mathrm{o}}R_{\mathrm{c}}}\right)$.

$$f_{\mathrm{R}_1}(r_1|v_{\mathrm{o}},R_{\mathrm{c}})=\begin{cases} f_{\mathrm{R}_1}^{(1)}(r_1|v_{\mathrm{o}},R_{\mathrm{c}})=\frac{2N_{\mathrm{s}}r_1}{R_{\mathrm{c}}^2}\left(1-\frac{r_1^2}{R_{\mathrm{c}}^2}\right)^{N_{\mathrm{s}}-1}, & 0\le r_1\le R_{\mathrm{c}}-v_{\mathrm{o}} \\ f_{\mathrm{R}_1}^{(2)}(r_1|v_{\mathrm{o}},R_{\mathrm{c}})=\frac{2N_{\mathrm{s}}r_1}{\pi R_{\mathrm{c}}^2}\arccos\left(\frac{r_1^2+v_{\mathrm{o}}^2-R_{\mathrm{c}}^2}{2v_{\mathrm{o}}r_1}\right) & \\ \quad\times\left(1-\left(\frac{r_1^2}{\pi R_{\mathrm{c}}^2}\left(\theta_1^1-\frac{1}{2}\sin\left(2\,\theta_1^1\right)\right)+\frac{1}{\pi}\left(\theta_2^1-\frac{1}{2}\sin\left(2\,\theta_2^1\right)\right)\right)\right)^{N_{\mathrm{s}}-1}, & R_{\mathrm{c}}-v_{\mathrm{o}}<r_1\le R_{\mathrm{c}}+v_{\mathrm{o}}, \end{cases} \tag{18}$$

with $\theta_1^1=\arccos\left(\frac{{r_1}^2-R_{\mathrm{c}}^2+v_{\mathrm{o}}}{2v_{\mathrm{o}}r_1}\right)$ and $\theta_2^1=\arccos\left(\frac{-{r_1}^2+R_{\mathrm{c}}^2+v_{\mathrm{o}}}{2v_{\mathrm{o}}R_{\mathrm{c}}}\right)$.

$$\begin{aligned} P_{\mathrm{c}}(\beta|v_{\mathrm{o}}) \;=\; & \int_0^{R_{\mathrm{c}}-v_0} f_{\mathrm{R}_1}^{(1)}(r_1|v_{\mathrm{o}},R_{\mathrm{c}})\left[\left[1-F_{\mathcal{H}}(\zeta_1,\rho)\right]\mathcal{P}_{\mathrm{L}}(r_1)+\left[1-F_{\mathcal{H}}(\zeta_1,\rho)\right]\mathcal{P}_{\mathrm{NL}}(r_1)\right]\mathrm{d}r_1 \\ & +\int_{\mathrm{R}_{\mathrm{c}}-\mathrm{v}_0}^{R_{\mathrm{c}}+v_0} f_{\mathrm{R}_1}^{(2)}(r_1|v_{\mathrm{o}},R_{\mathrm{c}})\left[\left[1-F_{\mathcal{H}}(\zeta_2,\rho)\right]\mathcal{P}_{\mathrm{L}}(r_1)+\left[1-F_{\mathcal{H}}(\zeta_2,\rho)\right]\mathcal{P}_{\mathrm{NL}}(r_1)\right]\mathrm{d}r_1, \end{aligned} \tag{21}$$

with $\zeta_1=\beta\sigma_{\mathrm{N}}^2[L_{\mathrm{L}}(r_1)]^2/P_{\mathrm{t}}\Gamma_{\mathrm{a}}$ and $\zeta_2=\beta\sigma_{\mathrm{N}}^2[L_{\mathrm{NL}}(r_1)]^2/P_{\mathrm{t}}\Gamma_{\mathrm{a}}$.

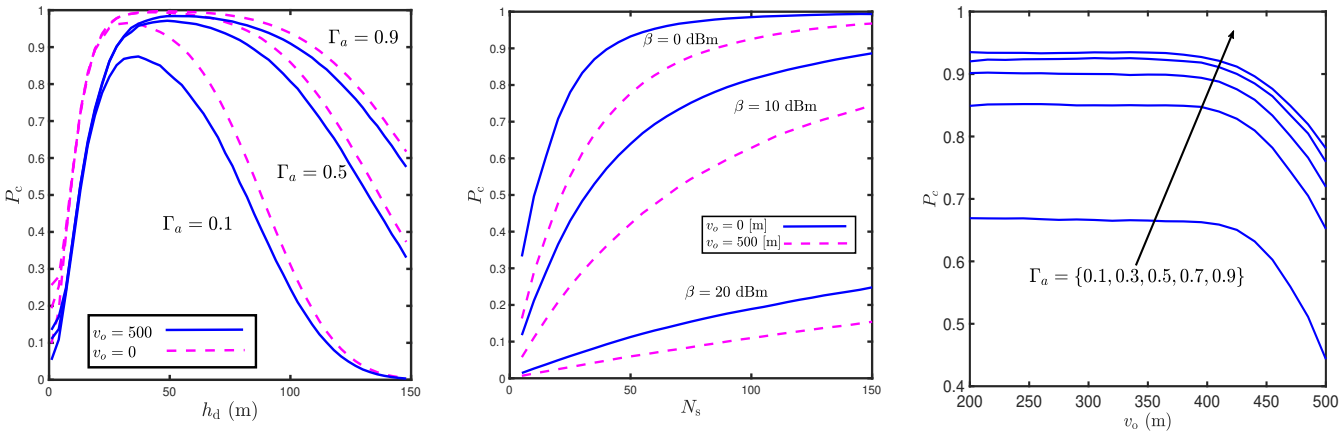

(a) (b) (c)

Fig. 5: (a) Coverage probability with $N_{\mathrm{s}}=200$, $R_{\mathrm{c}}=500$, $\rho=.5$, $\sigma_{\mathrm{N}}^2=-110$ dBm, $\beta=10$ dBm. (b) Coverage probability with $R_{\mathrm{c}}=500$, $\rho=.5$, $\sigma_{\mathrm{N}}^2=-110$ dBm, $\Gamma_{\mathrm{a}}=0.9$ and (c) Coverage probability with $h_{\mathrm{d}}=50$ [m], $N_{\mathrm{s}}=50$, $R_{\mathrm{c}}=500$, $\rho=.5$, $\sigma_{\mathrm{N}}^2=-110$ dBm, $\beta=0$ dBm.

DFR become closer to the border of the circular coverage area. This is due to the BPP non-stationarity (i.e., the distance distributions and void probability characteristics are not the same for any arbitrary chosen point). Lastly, Figure 6 investigates the effect of jointly changing the height of the DFR and the number of SNs on the coverage probability. The Figure

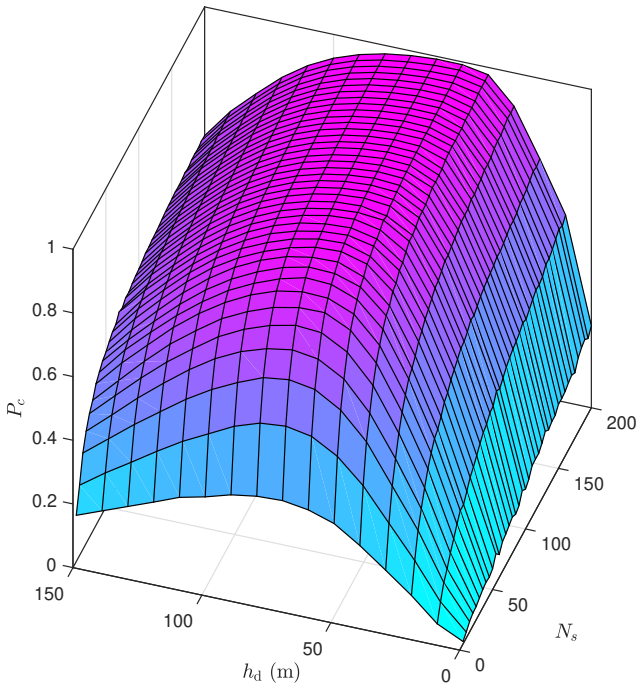

Fig. 6: Coverage probability. $R_{\mathrm{c}} = 500$, $\rho = .5$, $\sigma^2_{\mathrm{N}} = -110$ dBm, $\beta = 0$ dBm, $\Gamma_{\mathrm{a}} = 0.9$

shows that for any chosen number of SNs, there is always a DFR height that maximizes the coverage probability.

V. Conclusion

In this paper, we investigated design space of backscatter IoT SNs which are polled via drone based SN tag reader. We developed a point-to-point implementation using SDR and custom designed SN tag. We then developed a comprehensive statistical framework to quantify link level performance of randomly distributed SNs. Our model explicitly incorporates dyadic fading channel whereby forward (Drone-to-SN) and backward(SN-to-Drone) propagation channels can experience non-zero correlation. Performance analysis for dyadic fading channel is intricate due to nature of PDF expressions. We present closed-form tight approximations which simplify the analysis. Our analytical model also incorporates LoS and NLoS components which characterize the path-loss for drone based communication. The developed model is parametrized by the experimental implementation and subsequently impact of different parameters on the coverage performance of SN is investigated. We demonstrate that there exists a fruitful interplay between SN's reflection coefficient, drone height and number of SNs which jointly dictate an optimal operation point at which coverage probability is maximized.

References

[1] "State of the iot 2018: Number of iot devices now at 7b market accelerating." https://iot-analytics.com/state-of-the-iot-update-q1-q2-2018-number-of-iot-devices-now-7b/, [Online; accessed 17/03/2019].

[2] B. Clerckx, R. Zhang, R. Schober, D. W. K. Ng, D. I. Kim, and H. V. Poor, "Fundamentals of wireless information and power transfer: From rf energy harvester models to signal and system designs," *IEEE Journal on Selected Areas in Communications*, vol. 37, no. 1, pp. 4–33, 2019.

[3] V. Liu, A. Parks, V. Talla, S. Gollakota, D. Wetherall, and J. R. Smith, "Ambient backscatter: wireless communication out of thin air," in *ACM SIGCOMM Computer Communication Review*, vol. 43, pp. 39–50, ACM, 2013.

[4] A. Bletsas, P. N. Alevizos, and G. Vougioukas, "The art of signal processing in backscatter radio for μw (or less) internet of things: Intelligent signal processing and backscatter radio enabling batteryless connectivity," *IEEE Signal Processing Magazine*, vol. 35, no. 5, pp. 28–40, 2018.

[5] E. Kampianakis, J. Kimionis, K. Tountas, C. Konstantopoulos, E. Koutroulis, and A. Bletsas, "Wireless environmental sensor networking with analog scatter radio and timer principles," *IEEE Sensors Journal*, vol. 14, no. 10, pp. 3365–3376, 2014.

[6] C. Xu, L. Yang, and P. Zhang, "Practical backscatter communication systems for battery-free internet of things: A tutorial and survey of recent research," *IEEE Signal Processing Magazine*, vol. 35, no. 5, pp. 16–27, 2018.

[7] E. Kampianakis, J. Kimionis, K. Tountas, C. Konstantopoulos, E. Koutroulis, and A. Bletsas, "Backscatter sensor network for extended ranges and low cost with frequency modulators: Application on wireless humidity sensing," in *SENSORS, 2013 IEEE*, pp. 1–4, IEEE, 2013.

[8] S. N. Daskalakis, A. Collado, A. Georgiadis, and M. M. Tentzeris, "Backscatter morse leaf sensor for agricultural wireless sensor networks," in *2017 IEEE SENSORS*, pp. 1–3, IEEE, 2017.

[9] S.-N. Daskalakis, J. Kimionis, A. Collado, M. M. Tentzeris, and A. Georgiadis, "Ambient fm backscattering for smart agricultural monitoring," in *2017 IEEE MTT-S International Microwave Symposium (IMS)*, pp. 1339–1341, IEEE, 2017.

[10] A. M. Hayajneh, S. A. R. Zaidi, D. McLernon, and M. Ghogho, "Drone empowered small cellular disaster recovery networks for resilient smart cities," in *2016 First International Workshop on Toward A City-Wide Pervasive EnviRonment (SECON Workshops) (CoWPER'16)*, (London, United Kingdom), June 2016.

[11] A. M. Hayajneh, S. A. R. Zaidi, D. C. McLernon, M. Di Renzo, and M. Ghogho, "Performance analysis of uav enabled disaster recovery networks: A stochastic geometric framework based on cluster processes," *IEEE Access*, vol. 6, pp. 26215–26230, 2018.

[12] S. N. Chiu, D. Stoyan, W. S. Kendall, and J. Mecke, *Stochastic geometry and its applications*. John Wiley & Sons, 2013.

[13] K. Mueller and M. Muller, "Timing recovery in digital synchronous data receivers," *IEEE transactions on communications*, vol. 24, no. 5, pp. 516–531, 1976.

[14] M. Mozaffari, W. Saad, M. Bennis, and M. Debbah, "Drone small cells in the clouds: Design, deployment and performance analysis," *arXiv preprint arXiv:1509.01655*, 2015.

[15] Á. Baricz, "On a product of modified bessel functions," *Proceedings of the American Mathematical Society*, vol. 137, no. 1, pp. 189–193, 2009.

[16] M. Ahsanullah and V. B. Nevzorov, *Order statistics: examples and exercises*. Nova Publishers, 2005.